Clinical & Experimental Ophthalmology

RANZCO The Royal Australian and New Zealand College of Ophthalmologists

Clinical and Experimental Ophthalmology 2013; 41: 870–880 doi: 10.1111/ceo.12142

Original Article

Detection of macular ganglion cell loss in preperimetric glaucoma patients with localized retinal nerve fibre defects by spectral-domain optical coherence tomography

Jung Hwa Na MD,[1] Kyoungsub Lee MD,[1] Jong Rak Lee MD,[1] Seunghee Baek PhD,[2] Sung Jun Yoo BS[1] and Michael S Kook MD[1]

[1]Department of Ophthalmology, and [2]Department of Clinical Epidemiology and Biostatistics, College of Medicine, Asan Medical Center, University of Ulsan, Seoul, Korea

Abstract

Background: To evaluate and compare the utility of ganglion cell complex with peripapillary retinal nerve fibre layer and optic nerve head measurements for detection of localized defects in patients with preperimetric glaucoma using spectral-domain optical coherence tomography.

Design: Prospective study.

Participants: Preperimetric glaucoma patients.

Methods: A total of 105 eyes with preperimetric glaucoma and 68 age- and refractive error-matched control eyes were enrolled. The ability to detect localized retinal nerve fibre layer defects by RTVue-100 spectral-domain optical coherence tomography (Optovue, Inc., Fremont, CA, USA) was assessed calculating the areas under receiver operating characteristic curves.

Main Outcome Measures: The ability to detect localized retinal nerve fibre layer defects by spectral-domain optical coherence tomography.

Results: Global volume loss and superior ganglion cell complex thickness showed the largest area under receiver operating characteristic curve values (both areas under receiver operating characteristic curves 0.84, $P < 0.001$) among ganglion cell complex parameters. Average peripapillary retinal nerve fibre layer thickness afforded the best diagnostic capability (area under receiver operating characteristic curve 0.89, $P < 0.001$), whereas among optic nerve head parameters, the horizontal cup:disc ratio yielded the highest area under receiver operating characteristic curve (0.85, $P < 0.001$). No statistical difference was evident between the areas under receiver operating characteristic curves of the most informative parameters when the data were gathered from the three different sites (ganglion cell complex, peripapillary retinal nerve fibre layer, and optic nerve head) ($P > 0.02$).

Conclusions: Ganglion cell complex thickness was significantly reduced in eyes with preperimetric glaucoma. Ganglion cell complex imaging using spectral-domain optical coherence tomography may be a useful ancillary modality for detection of early macular changes in glaucomatous eyes with localized retinal nerve fibre layer defects.

Key words: ganglion cell complex, preperimetric glaucoma, spectral domain optical coherence tomography.

■ **Correspondence:** Prof. Michael S Kook, Department of Ophthalmology, University of Ulsan, College of Medicine, Asan Medical Center, 388-1 Pungnap-2-dong, Songpa-gu, Seoul 138-736, Korea. Email: mskook@amc.seoul.kr

Received 11 December 2012; accepted 22 April 2013.

Competing/conflicts of interest: No stated conflict of interest.

Funding sources: No stated funding sources.

Introduction

Glaucoma often starts with localized retinal nerve fibre layer (RNFL) defects without measurable visual field (VF) loss.[1–3] Red-free fundus photography has been established as the standard means of detecting glaucomatous RNFL defects in both qualitative and semiquantitative manner.[3–6] However, even the most sophisticated fundus photographs may sometimes be of limited clinical utility because image interpretation is qualitative and subjective.[7]

Introduction of spectral-domain optical coherence tomography (SD-OCT) has facilitated the segmentation and quantification of retinal layers because the technique offers high-level scan resolution and is rapid. Several recent studies have found that macular assessment has been shown to be a valuable surrogate measure when glaucomatous structural change is to be evaluated, and diagnostic accuracy was improved if macular assessment by SD-OCT focused on the inner retinal layers.[8–14] These inner layers have been arbitrarily termed the 'ganglion cell complex' (GCC); the complex can be readily viewed using RTVue-100 SD-OCT (Optovue, Inc., Fremont, CA, USA).

GCC measurements obtained using SD-OCT have been shown to afford better diagnostic accuracy and repeatability than do total macular thickness measurements derived using either time-domain OCT or SD-OCT.[15] Also, GCC thickness correlates strongly with peripapillary RNFL (pRNFL) thickness.[15,16] Previously, we reported that GCC thickness measurement afforded a glaucoma discrimination ability comparable with that of pRNFL thickness assessment in glaucomatous eyes with early VF defects or with VF defects close to the point of central fixation.[16] However, macular structural features in very early glaucomatous eyes remain poorly understood.

The objectives of the present study were to quantitatively assess the GCC structure of preperimetric glaucomatous eyes with localized RNFL defects using RTVue-100 SD-OCT and to investigate the capacity of GCC parameters to detect localized RNFL defects in comparison with measures of the pRNFL and optic nerve head (ONH).

Methods

Subjects

Patients with localized, glaucomatous RNFL defects attending our glaucoma clinic, but in whom standard automated perimetry (SAP) findings were normal, were consecutively enrolled between July 2010 and February 2011 at the Asan Medical Center, Seoul, Korea. Healthy control participants were also recruited. At initial evaluation, each subject underwent a complete ophthalmological examination in the same visit including the taking of medical, ocular and family histories; measurement of best-corrected visual acuity, refraction and axial length slit-lamp biomicroscopy; Goldmann applanation tonometry; gonioscopy, dilated fundoscopic examination using a 90- or 78-dioptre (D) lens; red-free fundus photography and stereoscopic optic disc photography; Humphrey field analysis (HFA) using the Swedish Interactive Threshold Algorithm 24-2 test (Carl Zeiss Meditec, Dublin, CA, USA); and RTVue-100 SD-OCT. For each patient, central corneal thickness was calculated as the average of three measurements obtained during the same visit using ultrasound pachymetry (DGH-550; DGH Technology, Inc., Exton, PA, USA).

All participants had to fulfil the following criteria for inclusion in the study: age >19 years; best-corrected visual acuity of 6/9 or better, with a spherical equivalent from −6 to +3 D and cylinder correction within +3 D, presence of a normal anterior chamber and open angle on slit-lamp and gonioscopic examinations, and reliable HFA test results with a false-positive error <15%, a false-negative error <15% and a fixation loss <20%.

All study participants showing localized RNFL defects on red-free fundus photography, as agreed upon by two glaucoma experts (MSK, JHN), underwent HFA testing twice. To minimize any learning effect, only the second HFA test result was used in analysis. Normal SAP result on the second HFA was required. A normal HFA test result was defined as the absence of a cluster of three points with a probability of less than 5% or a cluster of two points with a probability of less than 1% on the pattern deviation plot, and a glaucoma hemifield test result within normal limits.[17] One eye was randomly selected if both eyes were found to be eligible for the study. When one eye was preperimetric and the other normal, the preperimetric eye was selected.

Age- and refractive error-matched healthy eyes formed the control group. Control subjects consisted of staff and family members, patient spouses, and volunteers from the eye clinic and our hospital. All control eyes had an intraocular pressure lower than 22 mmHg, with no history of intraocular pressure elevation and were normal on VF examination using a single HFA test. The neuroretinal rim was intact, thus without disc haemorrhage, notches or any localized RNFL defect. All control subjects lacked RNFL defects, as confirmed by the same two specialists (MSK, JHN) upon study of red-free fundus photographs.

Patients with evidence of any intracranial or otolaryngeal lesion, a history of massive haemorrhage or hemodynamic crisis, any other ophthalmic disease that could affect ONH or RNFL evaluation, any condition that might bias SD-OCT measurements

(including severe peripapillary atrophy, chorioretinal coloboma and/or posterior staphyloma), or a history of diabetes mellitus or eye surgery/laser treatment were excluded.

All test procedures conformed to the tenets of the Declaration of Helsinki, and the study was approved by the Institutional Review Board of the Asan Medical Center at the University of Ulsan, Seoul, Korea. Informed consent was obtained from all subjects.

Red-free fundus photography

Red-free RNFL photographs were acquired using a digital fundus camera (TRC-50IX; Topcon, Tokyo, Japan, and MegaPlus 1.4i, Kodak, Rochester, New York, USA) after dilation of each pupil to a minimum diameter of 5 mm. Sixty-degree wide-angle views of the optic disc, sharply focused on the retina using an inbuilt split-line focusing device, were obtained and reviewed on an Liquid Crystal Display (LCD) monitor.[18–20]

All red-free fundus RNFL photographs were independently and randomly evaluated by two experienced observers (JHN, MSK) blinded to patient identity and clinical data. Each eye was classified as defect-free, with a localized defect (superior, inferior or both), with diffuse atrophy, or as ambiguous. This method has been described in detail elsewhere.[21,22] In brief, localized glaucomatous RNFL defects were considered to be present in red-free photographs if their width at a 1-disc-diameter distance from the edge of the disc was larger than a major retinal vessel and if they diverged in an arcuate or wedge shape reaching the edge of the disc. Diffuse defects are characterized by a generalized reduction in the normal striated pattern throughout the whole retina, and appear to blur into a uniform, dull, granular white-grey area. Eyes diagnosed with localized defects (superior, inferior or both) by both observers were eligible for inclusion in the study group.

Optical coherence tomography

SD-OCT was performed using RTVue software (version A4.0.5.100; Optovue, Inc.). The working principle of the device has been described in detail elsewhere.[23–26] Briefly, the ONH map modality involves performance of 12 radial scans each 3.4 mm in length, and 13 concentric ring scans ranging from 1.3 to 4.9 mm in diameter(centred on the optic disc). This scan configuration yields 14 141 A-scans in 0.55 s. A polar pRNFL thickness map of the 3.45-mm diameter ring and various parameters describing optic disc features are provided. The GCC scan measures retinal thickness between the posterior boundary of the inner plexiform layer and the anterior boundary of the RNFL. This protocol explores parameters within a ring scan diameter of 6 mm; the centre of the GCC scan is shifted 1 mm temporal to the fovea to improve sampling of temporal peripheral nerve fibres.

A normative database of GCC, pRNFL and ONH parameters has been developed via collection of data from normal eyes of individuals varying in race. The levels of statistical significance are shown in colour. Red indicates a probability $P < 0.01$, yellow $P < 0.05$ and green $P > 0.05$. Images with signal strength indices less than 45 on the ONH or GCC map, or showing overt decentration of measurement circle location (assessed subjectively), were excluded from analysis. All images were acquired by a single experienced operator (SJY). Pharmacological dilation was performed in all subjects to ensure optimal image quality and to permit careful retinal segmentation.

Statistical analysis

The Wilk–Shapiro test was used to examine the distribution of numerical data. Normally distributed data were compared between control subjects and preperimetric glaucoma patients employing unpaired *t*-tests. Non-parametric data were compared using the Mann–Whitney *U*-test. To compare categorical data, the chi-squared test was employed. To explore whether ONH and NFL (GCC and pRNFL) thickness parameters could discriminate between healthy and preperimetric glaucomatous eyes, areas under receiver operating characteristics curves (AUCs) were calculated and compared. Sensitivities at fixed specificities of 80%, 90% and 95% were also calculated from the AUCs. The DeLong method was used to evaluate statistical differences between AUCs yielded by different sites.[27] The Bonferroni correction was applied when AUC comparisons were performed to adjust for multiple testing.[28] A difference was considered significant at $P < 0.05$/number of comparisons ($n = 3$).

Likelihood ratios (LRs) of localized RNFL change detection using normative ONH and NFL thickness classifications were calculated. Jaeschke and colleagues[29] suggested the use of LRs to predict post-test disease probability. We interpreted the values of LRs according to their scheme, LRs higher than 10 or lower than 0.1 are associated with large effects on post-test probabilities; LRs from 5 to 10 or from 0.1 to 0.2, with moderate effects; LRs from 2 to 5 or from 0.2 to 0.5, with small effects; and LRs closer to 1 are insignificant. LRs for each category (5th–95th percentiles, green [within normal limits]; 1st–5th percentiles, yellow [borderline]; <1st percentile, red [abnormal]) were separately calculated. The 95%

Table 1. Baseline patient and control demographics (means ± standard deviations)

	Preperimetric glaucoma patients	Controls	*P* value
n (eyes)	105	68	
Gender (M/F)	59/46	27/41	0.043
Eye (OD/OS)	58/47	34/34	0.302
Age (years)	51.2 ± 10.7	52.3 ± 12.6	0.537
VA (decimal value)	0.9 ± 0.2	0.9 ± 0.2	0.590
SE (dioptres)	–0.89 ± 1.67	–0.61 ± 1.90	0.315
IOP (mmHg)	15.7 ± 3.7	15.3 ± 2.4	0.636
CCT (μm)	545 ± 28	551 ± 28	0.195
AL (mm)	24.2 ± 1.0	23.8 ± 1.1	0.071
MD (dB)	–0.34 ± 1.31	0.04 ± 1.09	0.041
PSD (dB)	1.63 ± 0.30	1.51 ± 0.33	0.012
RNFL defect location (Superior/Inferior/ both)	45/17/43	NA	
SSI of ONH map	61.8 ± 8.5	61.7 ± 9.3	0.944
SSI of GCC map	68.4 ± 7.9	67.9 ± 9.2	0.726

AL, axial length; CCT, central corneal thickness; IOP, intraocular pressure; GCC, ganglion cell complex; MD, mean deviation; NA, not applicable; ONH, optic nerve head; PSD, pattern standard deviation; RNFL, retinal nerve fibre layer; SE, spherical equivalent; SSI, signal strength index; VA, visual acuity.

confidence intervals of the LRs were also estimated. All *P* values were two-sided, and $P < 0.05$ was considered to reflect significance. Statistical analysis was performed using SPSS version 15.0 (SPSS, Inc., Chicago, IL, USA) and MedCalc version 9.6 (Mariakerke, Belgium).

Results

Of the 111 eyes that met our inclusion criteria, six were excluded because of unacceptable image quality (the signal strength index values of the ONH or GCC maps were <45). Finally, 105 eyes of 105 subjects were included in our preperimetric glaucoma group, and 68 healthy eyes of 68 subjects served as controls. All eyes were Asian. The baseline demographic characteristics of healthy controls and glaucoma patients are shown in Table 1. There was no significant difference in either mean age or refractive error between normal controls and patients with preperimetric RNFL defects (Table 1).

Upon measurement of both ONH and NFL (GCC and pRNFL) thickness, significant differences were evident, in all sectors, between healthy subjects and preperimetric glaucoma patients with localized RNFL defects, with the exception of the optic disc area (Table 2).

The AUCs and the AUC values for parameters derived from the scanning of the three distinct areas are shown in Figure 1 and Table 3. In terms of global NFL parameters, a significant difference was evident between average GCC and pRNFL thickness (AUCs 0.83 *vs.* 0.89, $P = 0.03$). However, for sectoral NFL thickness, no significant difference was apparent between GCC and pRNFL thickness values (AUCs 0.84 *vs.* 0.87, $P = 0.148$ for the superior sector; and 0.81 *vs.* 0.85, $P = 0.08$ for the inferior sector). The NFL and ONH parameters showing the highest sensitivities at a specificity of 95% were superior GCC (56.2%), average pRNFL (65.7%) and cup:disc area ratio (45.7%), respectively.

The AUCs for the most informative parameters (superior GCC thickness, average pRNFL thickness and the ONH horizontal cup:disc ratio) from the three different regions (GCC, pRNFL and ONH) were 0.84, 0.89 and 0.85, respectively. No statistically significant difference was evident after application of the Bonferroni correction to adjust for multiple testing ($P > 0.02$) (Fig. 1).

Table 4 shows the LRs obtained upon comparison with the inbuilt normative database. Results outside the normal limits for pRNFL parameters in terms of the global and sectoral averages and the 16 sectoral thicknesses had large effects on post-test glaucoma probability (infinite LRs). Similarly, results outside the normal limits for GCC parameters were associated with large effects on post-test glaucoma probability when either global or sectoral parameters were employed (infinite LRs). However, all ONH parameters (cup:disc area ratio, rim area and cup area) yielded small effect for outside the normal limits (LRs 3.89–5.11). Figure 2 illustrates a clinical example in which a localized RNFL defect associated with a normal SAP test result was detected by scanning using either the GCC or ONH map modality.

Discussion

First, we found that all parameters measured using the three scanning protocols differed significantly between healthy and glaucomatous eyes, except for

Table 2. Comparison of RTVue measurements on glaucomatous and normal patients (means ± standard deviations)

		Preperimetric glaucoma patients	Normal subjects	*P* value
pRNFL data (μm)				
16 sectors	TU1	65.2 ± 11.0	77.5 ± 8.8	<0.001
	TU2	84.8 ± 16.4	103.8 ± 12.4	<0.001
	ST2	112.2 ± 20.2	144.1 ± 16.9	<0.001
	ST1	121.6 ± 20.2	141.1 ± 23.4	<0.001
	SN1	104.7 ± 18.3	119.8 ± 20.3	<0.001
	SN2	105.9 ± 17.9	119.9 ± 17.2	<0.001
	NU2	86.0 ± 16.9	93.5 ± 14.6	0.002
	NU1	60.9 ± 111.7	67.3 ± 11.5	0.001
	NL1	57.8 ± 9.3	63.6 ± 12.0	0.002
	NL2	76.7 ± 13.6	86.6 ± 17.7	<0.001
	IN2	106.7 ± 18.4	122.7 ± 20.3	<0.001
	IN1	121.4 ± 20.6	143.0 ± 21.9	<0.001
	IT1	137.5 ± 20.3	164.0 ± 17.9	<0.001
	IT2	120.4 ± 24.6	141.4 ± 20.7	<0.001
	TL2	77.8 ± 12.7	88.0 ± 13.5	<0.001
	TL1	59.7 ± 9.8	66.7 ± 7.3	<0.001
Overall average		93.77 ± 8.95	109.03 ± 7.87	<0.001
Superior average		92.69 ± 10.46	108.66 ± 9.34	<0.001
Inferior average		94.87 ± 10.3	109.40 ± 9.24	<0.001
ONH parameters				
Rim volume (mm^3)		0.048 ± 0.060	0.123 ± 0.101	<0.001
Nerve head volume (mm^3)		0.097 ± 0.110	0.221 ± 0.148	<0.001
Cup volume (mm^3)		0.528 ± 0.319	0.289 ± 0.244	<0.001
Optic disc area (mm^2)		2.17 ± 0.63	2.02 ± 0.52	0.102
C:D area ratio		0.71 ± 0.17	0.46 ± 0.21	<0.001
Horizontal C:D ratio		0.92 ± 0.11	0.74 ± 0.20	<0.001
Vertical C:D ratio		0.84 ± 0.13	0.64 ± 0.20	<0.001
Rim area (mm^2)		0.60 ± 0.42	1.05 ± 0.39	<0.001
Cup area (mm^2)		1.57 ± 0.62	0.18 ± 0.37	<0.001
GCC parameters				
Overall average thickness (μm)		86.74 ± 6.52	95.58 ± 6.04	<0.001
Superior average thickness (μm)		86.81 ± 6.93	95.85 ± 6.05	<0.001
Inferior average thickness (μm)		86.58 ± 7.59	95.46 ± 6.38	<0.001
FLV (%)		2.255 ± 2.054	0.777 ± 0.838	<0.001
GLV (%)		14.099 ± 6.050	6.664 ± 4.189	<0.001

C:D, cup:disc ratio; FLV, focal loss volume; GCC, ganglion cell complex; GLV, global loss volume; IN, inferonasal sector; IT, inferotemporal sector; NL, lower nasal sector; NU, upper nasal sector; ONH, optic nerve head; pRNFL, peripapillary retinal nerve fibre layer; SN, superonasal sector; ST, superotemporal sector; TL, lower temporal sector; TU, upper temporal sector.

optic disc area. In the present study, the optimal parameters derived from each of the three scanned sites did not differ, with statistical significance, in terms of AUC. The GCC parameter showing the best performance, the superior average thickness, had a similar AUC (0.84) to that of pRNFL thickness (average pRNFL 0.89) and an ONH parameter (horizontal cup:disc ratio 0.85). However, the horizontal cup:disc ratio showed a lower sensitivity (45.7%) when specificity was set at 95%, compared with either average pRNFL (65.7%) or superior GCC (56.2%) thickness.

We found that pRNFL parameters generally yielded higher AUCs than did GCC parameters in terms of both global and sectoral thicknesses. The global pRNFL parameter (average pRNFL thickness 0.89) was significantly more sensitive than was the GCC parameter (average GCC 0.83). This is explained by the fact that the pRNFL scan examines almost all fibres arising from ganglion cells, whereas the GCC scan primarily samples the macular area. In addition, in the current study, eyes were recruited primarily by detection of RNFL defects contiguous with the superior and/or inferior optic disc margins, as shown on red-free fundus photography. This may have artefactually enhanced the sensitivity of pRNFL when used to detect preperimetric localized RNFL defects. In patients in whom ganglion cell loss occurs predominantly in the macula rather than at the periphery, GCC parameters may better detect earlier structural changes compared with pRNFL parameters.

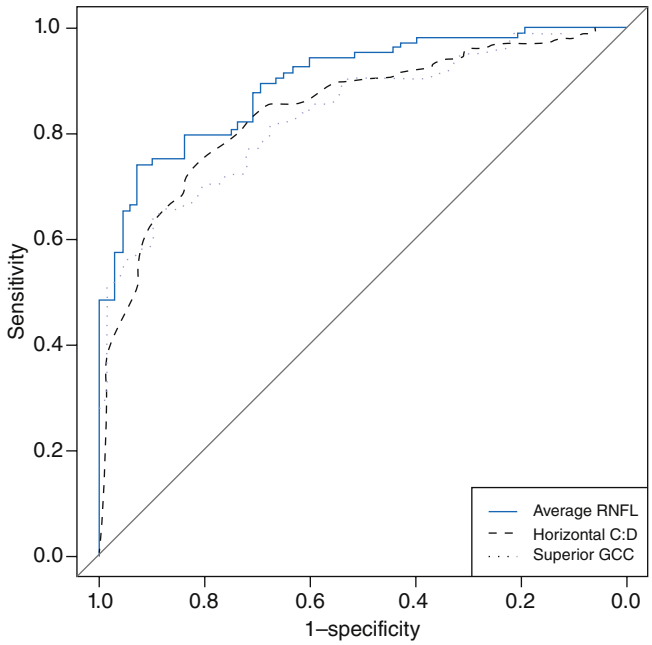

Figure 1. Comparisons of the area under receiver operating characteristic curves of the most informative parameters from three different areas of the eye. C:D, cup:disc ratio; GCC, ganglion cell complex; RNFL, retinal nerve fibre layer.

Notably, eyes with superotemporally localized RNFL defects were predominant in our consecutive series (45 superior *vs.* 17 inferior RNFL defects). This likely resulted in calculation of a higher superior GCC thickness AUC value compared with the AUC values of inferior or average GCC thicknesses. In terms of pRNFL data, our results are in line with previous findings,[30–32] indicating that average pRNFL thickness tended to be of greater diagnostic utility than was evaluation of sectoral pRNFL parameters.

Tan *et al.* explored the diagnostic utility of GCC parameters in a mixed (perimetric and preperimetric) glaucomatous group ($n = 130$); the cited authors used earlier RTVue SD-OCT methodology (software version, 3.0). The AUC of average GCC thickness was 0.78 in preperimetic subgroup ($n = 52$) defined by an abnormal appearance of the ONH.[15] Although direct comparisons among studies is problematic because of variations in equipment and study design, the AUC calculated in our current work is higher than that obtained by Tan *et al.* (0.83 vs. 0.78).[15] In addition, the cited authors reported that global loss volume (GCC-global loss volume) yielded an AUC value (0.79) slightly better than the average GCC (0.78).[15] Our current study of a larger series of preperimetric glaucoma patients revealed a similar trend in AUC values (GCC-global loss volume 0.84 *vs.* average GCC 0.83). In patients with localized RNFL defects, this pattern parameter may be more sensitive than is the GCC average value, as observed in our present study on patients in whom focal GCC loss predominated in the absence of any widespread macular structural change.

Notably, of the ONH parameters studied, the horizontal cup:disc ratio afforded the best diagnostic performance. Previous reports on ONH assessment using RTVue-100 found that the vertical cup:disc ratio yielded the highest AUC of all optic disc parameters evaluated in eyes with perimetric glaucoma.[9,12] The between-study discrepancies may be explained by differences in study design, including the imaging device/software employed, variation in sample size, and the extent of disease severity (perimetric *vs.* preperimetric). Alternatively, such differences may reflect the relatively poorer performance of RTVue-100 ONH software in terms of ONH topographic analysis compared with assessment of pRNFL or GCC thicknesses at early stages of optic nerve damage.

Previous studies[33,34] used clock-hour pRNFL thickness values yielded by Cirrus SD-OCT assessment, detailing the angular widths of localized RNFL defects calculated from evaluation of red-free RNFL photographs. In such case, no significant difference was evident between stratus and cirrus OCT evaluation in terms of detecting localized RNFL defects. In our current study, we did not measure the angular widths of localized RNFL defects, nor did we seek to evaluate the diagnostic powers of corresponding pRNFL sector(s) as defined by RTVue-100 because evaluation of red-free RNFL photographs is both subjective and qualitative. Notably, however, the ST2 sector yielded the largest AUC of all 16 sectors and most frequently hosted the localized RNFL defects observed on red-free fundus photography.

An LR value estimates how much a test result might change the likelihood of positive disease status. In our current study, the LRs for pRNFL and GCC thicknesses lying outside normal limits generally had large effects on post-test glaucoma probability. However, the LRs of ONH parameter values outside normal limits were associated with only small effects on such probabilities (LR values 3.89–5.11). This suggests that positive ONH data may be of limited utility in terms of confirmation of disease presence. However, the LR values for results within normal limits were not associated with a significant change at any of the three tested sites. In other words, such data are of limited utility if they are to be used to exclude disease.

The limitations of the current study include the use of a 'normal population' to define reference values and to determine diagnostic specificities. Inclusion of normal subjects based on normal optic nerve/RNFL appearance and standard VF test results on initial clinical examination tends to overestimate the diagnostic accuracy of the various RTVue-100

Table 3. AUCs and sensitivities at fixed specificities

		AUC (SE)	Cut-off value	Sensitivity	Specificity	Sensitivity/specificity		
						Specificity ≥80%	Specificity ≥90%	Specificity ≥95%
pRNFL parameter (μm)								
16 sectors	TU1	0.81 (0.03)	71	72.4	73.5	56.19/85.29	51.43/91.18	46.67/97.06
	TU2	0.82 (0.03)	93	70.5	82.4	71.43/80.88	58.1/91.18	53.33/95.59
	ST2	0.88 (0.03)	117	65.7	98.5	75.24/80.88	68.57/92.65	65.71/98.53
	ST1	0.75 (0.04)	131	68.6	70.6	45.71/80.88	31.43/92.65	15.24/95.59
	SN1	0.71 (0.04)	103	54.3	79.4	50.48/80.88	34.29/91.18	21.90/95.59
	SN2	0.71 (0.04)	108	60	73.5	51.43/80.88	33.33/91.18	20.95/95.59
	NU2	0.62 (0.04)	83	43.8	77.9	38.10/80.88	25.71/91.18	13.33/95.59
	NU1	0.64 (0.04)	56	39	83.8	39.05/83.82	20.95/92.65	16.19/95.59
	NL1	0.64 (0.05)	64	81	47.1	23.81/86.76	7.62/94.12	7.62/95.59
	NL2	0.66 (0.04)	85	73.3	54.4	35.24/80.88	15.24/92.65	9.52/95.59
	IN2	0.72 (0.04)	103	47.6	89.7	54.29/80.88	42.86/91.18	23.81/95.59
	IN1	0.77 (0.04)	138	83.8	58.8	51.43/82.35	29.52/91.18	24.76/97.06
	IT1	0.83 (0.03)	145	72.4	80.9	72.38/80.88	52.38/92.65	43.81/97.06
	IT2	0.74 (0.04)	116	50.5	91.2	55.24/82.35	50.48/91.18	42.86/95.59
	TL2	0.72 (0.04)	78	61.9	75	51.43/82.35	35.24/91.18	20.95/95.59
	TL1	0.73 (0.04)	62	64.8	70.6	53.33/80.88	38.10/91.18	32.38/97.06
Overall average		0.89 (0.02)	99.2	74.3	92.6	80.00/83.82	74.29/92.65	65.71/95.59
Superior average		0.87 (0.03)	100.3	79	82.4	80.0/80.88	66.67/91.18	50.48/97.06
Inferior average		0.85 (0.03)	98.2	65.7	89.7	72.38/82.35	61.90/92.65	55.24/95.59
ONH parameters								
Rim volume (mm^3)		0.84 (0.03)	0.049	75.2	80.9	75.24/80.88	55.24/91.18	38.10/95.59
Nerve head volume (mm^3)		0.83 (0.03)	0.115	79	76.5	72.38/80.88	55.24/91.18	40.95/95.59
Cup volume (mm^3)		0.73 (0.04)	0.384	64.8	72.1	50.48/80.88	37.14/91.18	15.24/95.59
Optic disc area (mm^2)		0.57 (0.04)	2	63.8	57.4	35.24/80.88	15.24/91.18	7.62/95.59
C:D area ratio		0.84 (0.03)	0.63	81	79.4	77.14/80.88	57.14/86.76	45.71/92.65
Horizontal C:D ratio		0.85 (0.03)	0.9	72.4	82.4	72.38/82.35	60.95/91.18	45.71/95.59
Vertical C:D ratio		0.83 (0.03)	0.8	73.3	82.4	74.29/80.88	47.62/91.18	38.10/95.59
Rim area (mm^2)		0.83 (0.03)	0.65	66.7	86.8	72.38/80.88	53.33/92.65	43.81/97.06
Cup area (mm^2)		0.76 (0.04)	1.27	65.7	76.5	56.19/80.88	45.71/91.18	39.05/95.59
GCC parameters								
Overall average (μm)		0.83 (0.03)	93.37	88.57	61.76	63.81/80.88	55.24/91.18	52.38/95.59
Superior average (μm)		0.84 (0.03)	88.9	64.8	89.7	70.48/80.88	58.10/92.65	56.19/95.59
Inferior average (μm)		0.81 (0.03)	93.48	83.8	63.2	60.95/82.35	55.24/91.18	48.57/95.59
FLV (%)		0.75 (0.04)	2.387	41.9	97.1	51.43/80.88	43.81/92.65	42.86/95.59
GLV (%)		0.84 (0.03)	7.68	87.6	63.2	61.9/85.29	57.14/91.18	48.57/97.06

AUC, area under receiver operating characteristic curve; C:D, cup-disc; FLV, focal loss volume; GLV, global loss volume; IN, inferonasal sector; IT, inferotemporal sector; GCC, ganglion cell complex; ONH, optic nerve head; NL, lower nasal sector; NU, upper nasal sector; pRNFL, peripapillary retinal nerve fibre layer; SN, superonasal sector; ST, superotemporal sector; TL, lower temporal sector; TU, upper temporal sector.

Table 4. Likelihood ratios of RTVue spectral-domain optical coherence tomography parameters (95% confidence intervals)

		Within normal limits	Borderline	Outside normal limits
pRNFL parameters (μm				
16 sectors	TU1	0.705 (0.623–0.798)	I (NA–I)	I (NA-I)
	TU2	0.562 (0.475–0.665)	I (NA–I)	I (NA-I)
	ST2	0.483 (0.395–0.592)	16.838 (2.339–121.212)	I (NA-I)
	ST1	0.688 (0.590–0.802)	4.210 (1.537–11.529)	I (NA-I)
	SN1	0.717 (0.624–0.825)	5.397 (1.695–17.182)	I (NA-I)
	SN2	0.710 (0.606–0.833)	2.590 (1.117–6.006)	I (NA-I)
	NU2	0.863 (0.768–0.970)	2.202 (0.852–5.690)	I (NA-I)
	NU1	0.857 (0.773–0.950)	3.886 (1.190–12.691)	I (NA-I)
	NL1	0.955 (0.841–1.085)	1.223 (0.579–2.585)	I (NA-I)
	NL2	0.911 (0.826–1.005)	2.105 (0.716–6.188)	I (NA-I)
	IN2	0.773 (0.692–0.864)	14.248 (1.966–103.263)	I (NA-I)
	IN1	0.805 (0.721–0.898)	4.857 (1.147–20.573)	I (0.605-I)
	IT1	0.648 (0.559–0.750)	12.952 (1.779–94.290)	I (1.427-I)
	IT2	0.638 (0.543–0.749)	4.965 (1.551–15.899)	I (NA-I)
	TL2	0.877 (0.795–0.967)	3.670 (1.118–12.050)	I (NA-I)
	TL1	0.847 (0.762–0.941)	3.454 (1.046–11.408)	I (NA-I)
Overall average		0.399 (0.311–0.511)	7.340 (2.347–2.958)	I (NA–I)
Superior average		0.445 (0.353–0.562)	4.371 (1.600–11.940)	I (NA–I)
Inferior average		0.503 (0.413–0.611)	14.895 (2.059–107.750)	I (NA–I)
ONH parameters				
C:D area ratio		0.441 (0.317–0.6113)	1.245 (0.686–2.262)	3.886 (1.962–7.697)
Rim area (mm^2)		0.259 (0.170–0.394)	1.490 (0.757–2.931)	5.109 (2.568–9.810)
Cup area (mm^2)		0.261 (0.172–0.396)	1.491 (0.757–2.932)	5.105 (2.567–9.799)
GCC parameters				
Overall average (μm)		0.463 (0.367–0.583)	3.886 (1.586–9.522)	I (NA–I)
Superior average (μm)		0.438 (0.348–0.552)	6.908 (2.202–21.674)	I (NA–I)
Inferior average (μm)		0.505 (0.399–0.639)	2.015 (1.014–4.002)	I (NA–I)
FLV (%)		0.607 (0.509–0.724)	2.590 (0.759–8.843)	21.371 (2.993–152.627)
GLV (%)		0.368 (0.262–0.517)	0.648 (0.356–1.179)	I (NA–I)

C:D, cup-to-disc; FLV, focal loss volume; GLV, global loss volume; I, infinity; IN, inferonasal sector; IT, inferotemporal sector; GCC, ganglion cell complex; ONH, optic nerve head; NA, not applicable; NL, lower nasal sector; NU, upper nasal sector; pRNFL, peripapillary retinal nerve fibre layer; SN, superonasal sector; ST, superotemporal sector; TL, lower temporal sector; TU, upper temporal sector, NA-not applicable.

OCT modes tested. However, such limitations are common to all case-control studies. Another limitation is that this study uses a structural criterion (red-free wedge defect) to evaluate the sensitivity of a different structural measure (SD-OCT measurements). This will artificially increase the sensitivity of the RTVue-100 OCT. However, our goal of current study was to test discriminating ability of SD-OCT against preperimetric glaucoma (structural damage without functional impairment) as defined by wedge-shape defect on red-free photography. All patients and controls were Asian (Korean) by race, and our data may thus not be automatically generalized to other races. Although all our patients had preperimetric glaucoma based on red-free photography with normal SAP finings, there was a significant difference between the two groups with respect to Mean deviation (MD) and pattern standard deviation. Therefore, it is possible that these patients could have macular damage secondary to glaucoma that was not visible with SAP. The statistical literature does not currently contain a consensus on significance values obtained using multiple comparisons; the use of various AUC values in terms of diagnostic performance is subject to this conceptual constraint.[35–39] In our current study, in which we compared diagnostic performances afforded by measures taken at different sites within the eye, stringent tests (including Bonferroni adjustment) were applied in an effort to strictly validate our among-test comparisons. Additionally, pupil dilation was performed in all of our participants to avoid influence of different pupil state. It may affect image quality and diagnostic sensitivity. However, it was found that there was no clinical significant thickness change in pRNFL and GCC in RTVue-100 OCT because of pupil dilation.[24] Thus, we believe that our results can be applied in routine clinics where pupil dilation is not regularly performed before imaging. Recently, higher version of RTVue-100 OCT software was introduced, new software version employs less RNFL sectors with wider size than our study version

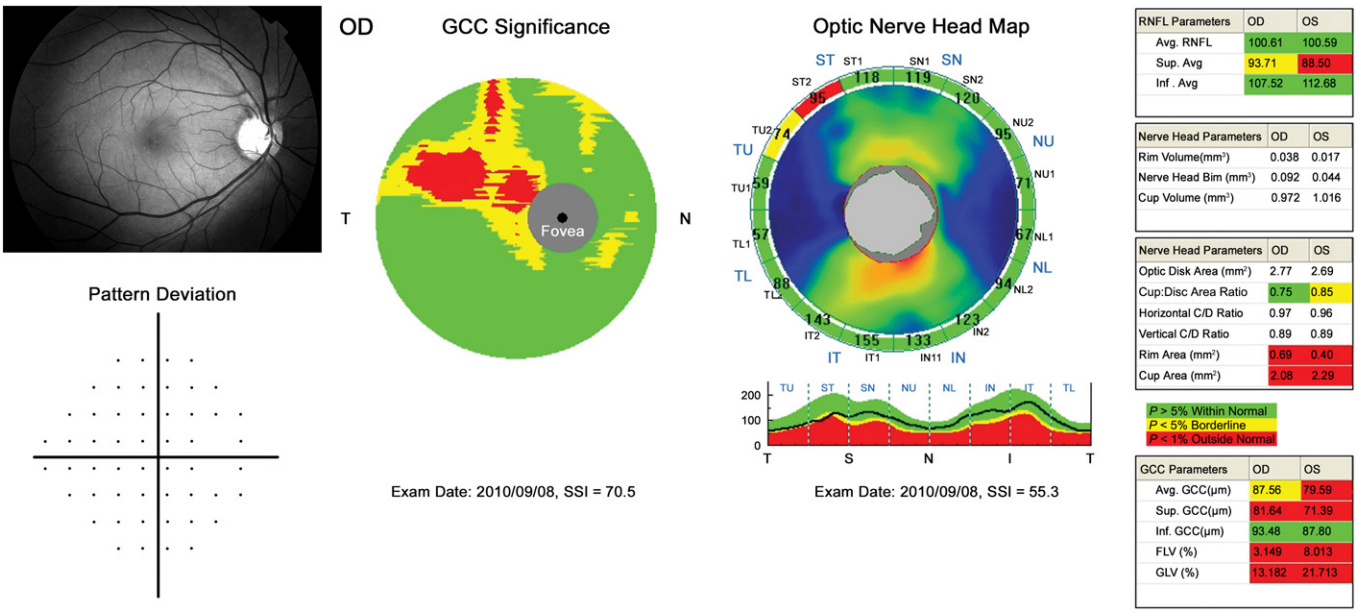

Figure 2. A right eye showing a superior localized retinal nerve fibre layer (RNFL) defect on red-free fundus photography, but a normal visual field. RTVue optical coherence tomography measurements revealed that both the optic nerve head and ganglion cell complex (GCC) significance maps reported abnormal findings. C:D, cup:disc ratio; IN, inferonasal sector; IT, inferotemporal sector; OD, right eye; OS, left eye; SN, superonasal sector; ST, superotemporal sector; TL, lower temporal sector; TU, upper temporal sector.

(version 4.0) does. It was reported that new version (version 6.3) decreases the probability of detection of narrow focal RNFL defects in glaucoma.[40] Therefore, our results might not be replicated when higher software version is used. Finally, myopia is one of the risk factors of glaucoma[41,42] and is highly prevalent in East Asia.[43,44] However, in highly myopic eyes, it is difficult to precisely diagnose glaucoma. Previously, it was reported that RTVue-100 OCT was useful for discriminating perimetric glaucoma with high myopia.[45] Current study included participants with refractive error from −6 to +3 D. Therefore, further studies are needed whether our results can be applied on highly myopic eyes with preperimetric glaucoma.

In conclusion, GCC thickness was significantly reduced in eyes with localized RNFL defects and normal SAP. The ability to detect localized RNFL defects using the most informative GCC parameter did not differ significantly from that afforded by pRNFL or ONH data. Macular imaging via use of SD-OCT may be a useful adjunct mode for detection of early macular structural changes even in patients with preperimetric glaucoma and localized RNFL defects.

References

1. Horn FK, Jonas JB, Martus P, Mardin CY, Budde WM. Polarimetric measurement of retinal nerve fiber layer thickness in glaucoma diagnosis. *J Glaucoma* 1999; **8**: 353–62.
2. Quigley HA, Katz J, Derick RJ, Gilbert D, Sommer A. An evaluation of optic disc and nerve fiber layer examinations in monitoring progression of early glaucoma damage. *Ophthalmology* 1992; **99**: 19–28.
3. Sommer A, Katz J, Quigley HA *et al.* Clinically detectable nerve fiber atrophy precedes the onset of glaucomatous field loss. *Arch Ophthalmol* 1991; **109**: 77–83.
4. Sommer A, Miller NR, Pollack I, Maumenee AE, George T. The nerve fiber layer in the diagnosis of glaucoma. *Arch Ophthalmol* 1977; **95**: 2149–56.
5. Zangwill LM, Williams J, Berry CC, Knauer S, Weinreb RN. A comparison of optical coherence tomography and retinal nerve fiber layer photography for detection of nerve fiber layer damage in glaucoma. *Ophthalmology* 2000; **107**: 1309–15.
6. Quigley HA. Examination of the retinal nerve fiber layer in the recognition of early glaucoma damage. *Trans Am Ophthalmol Soc* 1986; **84**: 920–66.
7. Lichter PR. Variability of expert observers in evaluating the optic disc. *Trans Am Ophthalmol Soc* 1976; **74**: 532–72.
8. Garas A, Vargha P, Hollo G. Diagnostic accuracy of nerve fibre layer, macular thickness and optic disc measurements made with the RTVue-100 optical coherence tomograph to detect glaucoma. *Eye (Lond)* 2011; **25**: 57–65.
9. Huang JY, Pekmezci M, Mesiwala N, Kao A, Lin S. Diagnostic power of optic disc morphology, peripapillary retinal nerve fiber layer thickness, and macular inner retinal layer thickness in glaucoma diagnosis

with fourier-domain optical coherence tomography. *J Glaucoma* 2011; **20**: 87–94.
10. Ishikawa H, Stein DM, Wollstein G, Beaton S, Fujimoto JG, Schuman JS. Macular segmentation with optical coherence tomography. *Invest Ophthalmol Vis Sci* 2005; **46**: 2012–7.
11. Kotera Y, Hangai M, Hirose F, Mori S, Yoshimura N. Three-dimensional imaging of macular inner structures in glaucoma by using spectral-domain optical coherence tomography. *Invest Ophthalmol Vis Sci* 2011; **52**: 1412–21.
12. Rao HL, Zangwill LM, Weinreb RN, Sample PA, Alencar LM, Medeiros FA. Comparison of different spectral domain optical coherence tomography scanning areas for glaucoma diagnosis. *Ophthalmology* 2010; **117**: 1692–9. 9.e1.
13. Tan O, Li G, Lu AT, Varma R, Huang D. Mapping of macular substructures with optical coherence tomography for glaucoma diagnosis. *Ophthalmology* 2008; **115**: 949–56.
14. Nakatani Y, Higashide T, Ohkubo S, Takeda H, Sugiyama K. Evaluation of macular thickness and peripapillary retinal nerve fiber layer thickness for detection of early glaucoma using spectral domain optical coherence tomography. *J Glaucoma* 2010; **20**: 252–9.
15. Tan O, Chopra V, Lu AT *et al*. Detection of macular ganglion cell loss in glaucoma by Fourier-domain optical coherence tomography. *Ophthalmology* 2009; **116**: 2305–14. e1–2.
16. Seong M, Sung KR, Choi EH *et al*. Macular and peripapillary retinal nerve fiber layer measurements by spectral domain optical coherence tomography in normal-tension glaucoma. *Invest Ophthalmol Vis Sci* 2010; **51**: 1446–52.
17. Caprioli J. Automated perimetry in glaucoma. *Am J Ophthalmol* 1991; **111**: 235–9.
18. Hoyt WF, Frisen L, Newman NM. Fundoscopy of nerve fiber layer defects in glaucoma. *Invest Ophthalmol* 1973; **12**: 814–29.
19. Richards DW, Janesick JR, Elliot ST *et al*. Enhanced detection of normal retinal nerve-fiber striations using a charge-coupled device and digital filtering. *Graefes Arch Clin Exp Ophthalmol* 1993; **231**: 595–9.
20. Wang F, Quigley HA, Tielsch JM. Screening for glaucoma in a medical clinic with photographs of the nerve fiber layer. *Arch Ophthalmol* 1994; **112**: 796–800.
21. Pablo LE, Ferreras A, Schlottmann PG. Retinal nerve fibre layer evaluation in ocular hypertensive eyes using optical coherence tomography and scanning laser polarimetry in the diagnosis of early glaucomatous defects. *Br J Ophthalmol* 2011; **95**: 51–5.
22. Quigley HA, Reacher M, Katz J, Strahlman E, Gilbert D, Scott R. Quantitative grading of nerve fiber layer photographs. *Ophthalmology* 1993; **100**: 1800–7.
23. Gonzalez-Garcia AO, Vizzeri G, Bowd C, Medeiros FA, Zangwill LM, Weinreb RN. Reproducibility of RTVue retinal nerve fiber layer thickness and optic disc measurements and agreement with Stratus optical coherence tomography measurements. *Am J Ophthalmol* 2009; **147**: 1067–74. 74.e1.
24. Garas A, Vargha P, Hollo G. Reproducibility of retinal nerve fiber layer and macular thickness measurement with the RTVue-100 optical coherence tomograph. *Ophthalmology* 2010; **117**: 738–46.
25. Garas A, Toth M, Vargha P, Hollo G. Comparison of repeatability of retinal nerve fiber layer thickness measurement made using the RTVue Fourier-domain optical coherence tomograph and the GDx scanning laser polarimeter with variable or enhanced corneal compensation. *J Glaucoma* 2010; **19**: 412–7.
26. Garas A, Vargha P, Hollo G. Automatic, operator-adjusted, and manual disc-definition for optic nerve head and retinal nerve fiber layer measurements with the RTVue-100 optical coherence tomograph. *J Glaucoma* 2011; **20**: 80–6.
27. DeLong ER, DeLong DM, Clarke-Pearson DL. Comparing the areas under two or more correlated receiver operating characteristic curves: a nonparametric approach. *Biometrics* 1988; **44**: 837–45.
28. Lambers Heerspink HJ, Gansevoort RT, Brenner BM *et al*. Comparison of different measures of urinary protein excretion for prediction of renal events. *J Am Soc Nephrol* 2010; **21**: 1355–60.
29. Jaeschke R, Guyatt GH, Sackett DL. Users' guides to the medical literature. III. How to use an article about a diagnostic test. B. What are the results and will they help me in caring for my patients? The Evidence-Based Medicine Working Group. *JAMA* 1994; **271**: 703–7.
30. Ferreras A, Pablo LE, Pajarin AB, Larrosa JM, Polo V, Honrubia FM. Logistic regression analysis for early glaucoma diagnosis using optical coherence tomography. *Arch Ophthalmol* 2008; **126**: 465–70.
31. Huang ML, Chen HY. Development and comparison of automated classifiers for glaucoma diagnosis using stratus optical coherence tomography. *Invest Ophthalmol Vis Sci* 2005; **46**: 4121–9.
32. Medeiros FA, Zangwill LM, Bowd C, Vessani RM, Susanna R, Weinreb RN. Evaluation of retinal nerve fiber layer, optic nerve head, and macular thickness measurements for glaucoma detection using optical coherence tomography. *Am J Ophthalmol* 2005; **139**: 44–55.
33. Jeoung JW, Park KH. Comparison of cirrus OCT and stratus OCT on the ability to detect localized retinal nerve fiber layer defects in preperimetric glaucoma. *Invest Ophthalmol Vis Sci* 2010; **51**: 938–45.
34. Kim NR, Lee ES, Seong GJ, Choi EH, Hong S, Kim CY. Spectral-domain optical coherence tomography for detection of localized retinal nerve fiber layer defects in patients with open-angle glaucoma. *Arch Ophthalmol* 2010; **128**: 1121–8.
35. Perneger TV. What's wrong with Bonferroni adjustments. *BMJ* 1998; **316**: 1236–8.
36. Rothman KJ. No adjustments are needed for multiple comparisons. *Epidemiology* 1990; **1**: 43–6.
37. Sankoh AJ, Huque MF, Dubey SD. Some comments on frequently used multiple endpoint adjustment methods in clinical trials. *Stat Med* 1997; **16**: 2529–42.

38. Savitz DA, Olshan AF. Multiple comparisons and related issues in the interpretation of epidemiologic data. *Am J Epidemiol* 1995; **142**: 904–8.
39. Zhang J, Quan H, Ng J, Stepanavage ME. Some statistical methods for multiple endpoints in clinical trials. *Control Clin Trials* 1997; **18**: 204–21.
40. Naghizadeh F, Holló G. Influence of software upgrade on detection of localized nerve fiber defects with the RTVue optical coherence tomograph in glaucoma. *Eur J Ophthalmol* 2012; **23**: 423–6.
41. Mitchell P, Hourihan F, Sandbach J, Wang JJ. The relationship between glaucoma and myopia: the Blue Mountains Eye Study. *Ophthalmology* 1999; **106**: 2010–5.
42. Suzuki Y, Iwase A, Araie M *et al.* ; Tajimi Study Group. Risk factors for open-angle glaucoma in a Japanese population: the Tajimi Study. *Ophthalmology* 2006; **113**: 1613–7.
43. Sawada A, Tomidokoro A, Araie M, Iwase A, Yamamoto T, Tajimi Study Group. Refractive errors in an elderly Japanese population: the Tajimi study. *Ophthalmology* 2008; **115**: 363–70.
44. Yoon KC, Mun GH, Kim SD *et al.* Prevalence of eye diseases in South Korea: data from the Korea National Health and Nutrition Examination Survey 2008–2009. *Korean J Ophthalmol* 2011; **25**: 421–33.
45. Shoji T, Sato H, Ishida M, Takeuchi M, Chihara E. Assessment of glaucomatous changes in subjects with high myopia using spectral domain optical coherence tomography. *Invest Ophthalmol Vis Sci* 2011; **52**: 1098–102.